Korean J. Chem. Eng., 37(9), 1552-1564 (2020)
DOI: 10.1007/s11814-020-0535-0

pISSN: 0256-1115
eISSN: 1975-7220

Improvement in separation performance of PEI-based nanofiltration membranes by using L-cysteine functionalized POSS-TiO_2 composite nanoparticles for removal of heavy metal ion

Samaneh Bandehali*, Fahime Parvizian*, Abdolreza Moghadassi*,†, Jiangnan Shen, and Sayed Mohsen Hosseini*,†**

*Department of Chemical Engineering, Faculty of Engineering, Arak University, Arak 38156-8-8349, Iran
**Center for Membrane Separation and Water Science & Technology, Ocean College,
Zhejiang University of Technology, Hangzhou 310014, China
(*Received 25 November 2019 • Revised 5 March 2020 • Accepted 8 March 2020*)

Abstract−L-cysteine as an amino acid was used for the modification of glycidyl POSS in the synthesis of L-cysteine functionalized POSS, including carboxyl, hydroxyl, and diamine groups. Then, the synthesized nanoparticles were applied to fabrication of L-cysteine POSS-TiO_2 composite nanoparticles. NF membranes were prepared from the incorporation of different concentrations of the synthesized composite nanoparticles into the polyether-imide (PEI) as the membrane matrix. The prepared membranes were characterized by Fourier transform infrared spectroscopy (FTIR), Field emission scanning electron microscopy (FESEM) and atomic force microscope (AFM). Moreover, the separation performance of the NF membranes was examined by pure water flux (PWF) and the separation of Na_2SO_4, $Pb(NO_3)_2$, $Cr(NO_3)_2$ and $Cu(NO_3)_2$ aqueous solutions. The results showed the increase of pure water flux due to present hydrophilic groups on the membrane surface. The highest pure water flux obtained was 22.03 L/m^2h in 1 wt% of nanoparticles. Furthermore, the rejection of Na_2SO_4 and $Pb(NO_3)_2$, $CrSO_4$, and $Cu(NO_3)_2$ improved to 78%, 64%, 67% and 66% that increased 11%, 33%, and 22%, and 39% compared with the pristine PEI membrane, respectively. Finally, the best FRR% (81%) was obtained for 0.1 wt% of the composite nanoparticles (M3).

Keywords: Polyether-imide, Nanofiltration, L-cysteine/POSS-TiO_2, Composite Nanoparticles, Heavy Metal Ions

INTRODUCTION

Nanofiltration (NF) membranes have gained much attention for wastewater treatment due to their high separation performance in monovalent and multivalent salts removal. The greatest challenge for the enhancement of NF membranes is the achievement of high pure water flux without decreasing salt rejection and good antifouling properties [1-3]. Membrane fouling on the membrane surface occurs due to the aggregation of pollutants, which reduces the separation performance of NF membranes. There are different methods to overcome these challenges and improvement of separation performance such as surface modification of membrane, grafting, cross-linking, coating, and incorporation of organic and inorganic materials [4-7]. Among these methods, the use of hydrophilic nanomaterials such as carbon nanotubes (CNTs), graphene oxide (GO), and metal oxides into the polymer structure is a common method for improvement of NF membrane separation performance [8-11]. But nanoparticle aggregation and reducing compatibility between polymer and nanoparticles leads to creating nonselective voids and decreases the membrane performance. One method for better dispersion and more affinity between polymer and nanoparticles is the construction of new nanomaterials, including suitable functional groups [12].

In this study, a novel composite nanomaterial was synthesized by combination of TiO_2 and polyhedral oligomeric silsesquioxane (POSS) nanoparticles. The TiO_2 nanoparticles have high stability, non-toxicity, photo-catalytic, and good hydrophilic properties [13-15]. Moreover, POSS nanoparticles have a unique structure with high flexibility which makes possible its functionalization easily. This provides better affinity for them with membrane matrix [16-18]. There are many studies for the application of POSS in membranes gas separation and pervaporation [19-22]. Moreover, some studies focused on the metal ion removal from aqueous solutions by POSS nanomaterials due to cage structure and its high capacity for heavy metal adsorption [23,24]. Also, several studies considered POSS nanomaterials in membranes for wastewater treatment that reported improvement of separation properties and their yield such as overcoming to the membrane clogging, as well as their accumulation at high concentrations of nanoparticles. For example, You et al. [25] reported the functionalization of POSS nanoparticles with polyethylene glycol (PEG). These nanoparticles were applied to preparing polyamide (PA)-based membranes by interfacial polymerization. The membrane hydrophilicity and electronegativity of fabricated membranes was enhanced compared with the pristine PA membrane. The best separation performance was obtained for 0.5 wt% of PEG-POSS nanoparticles with PWF of 38.7 ($Lm^{-2}h^{-1}$) and Na_2SO_4 rejection about 90%. Moreover, the flux recovery ratio reached 98%. In another work, You et al. [18] showed the application of amine-functionalized POSS nanoparticles for the achievement of pore tuning in polydopamine (PDA)

†To whom correspondence should be addressed.
E-mail: a-moghadassi@araku.ac.ir, s-hosseini@araku.ac.ir

membrane with a mean pore size of 1.04-1.07 nm. The water permeability reached 1,099 $Lm^{-2}h^{-1}MPa^{-1}$. Moreover, cross-linking between POSS and PDA increased the resistance of compaction and reinforced alkali. He et al. [17] fabricated the NF membranes from polyamide and POSS for heavy metals (selenium and arsenic) separation. Dalwani et al. [26] fabricated thin film from POSS-polyamide by interfacial polycondensation of POSS with acyl chloride. These thin films were robust and flexible and showed high selectivity in liquid permeation. Chen et al. [27] fabricated hollow fiber membranes from polybenzimidazole (PBI)-POSS/polyacrylonitrile (PAN) for the application in forward osmosis (FO) and pressure retarded osmosis (PRO) processes. They studied two types of membrane fouling: inorganic fouling ($CaSO_4 \cdot 2H_2O$ gypsum scaling) during FO operations and organic fouling (sodium alginate fouling) during PRO operations. The results revealed that gypsum scaling on the membrane surface may be inhibited and even eliminated with an increment in reverse $MgCl_2$ flux due to competitive formations of $MgSO_4$ and $CaSO_4 \cdot 2H_2O$. In contrast, the increase of reverse NaCl flux exhibits a slight enhancement in alginate fouling in both FO and PRO processes. Compared to the reverse salt flux, the permeate flux always plays a dominant role in fouling. Therefore, lesser fouling has been observed on the membrane surface under the pressurized PRO process than FO process, because the reduced initial flux mitigates fouling phenomena more significantly than the enhancement caused by an increase in reverse NaCl flux.

Duan et al. [28] fabricated thin-film nano-composites (TFN) membranes from polyamide (PA) for reverse osmosis by POSS as nanofillers. POSS particles were incorporated on the selective layer via interfacial polymerization. Thin film nanocomposite membranes containing of 0.4% (w/v) P-8Phenylin showed a 65% increment in water flux compared to the pristine PA membrane without decline in high salt rejection. The thin film nanocomposite membranes with monoamine P-1NH_2 showed low pure water flux 3.2 $L/m^2 \cdot h$. P-8NH_3Cl showed the highest pure water flux (35.4 $L/m^2 \cdot h$) at 1% triethylamine (TEA). Lu et al. [29] used one-step electrospinning technique by the fluorinated-decyl polyhedraloligomeric silsesquioxane (F-POSS) colloidal suspension solution and PVDF-HFP for the preparation of omniphobic nanofiber membrane for membrane distillation (MD). These membranes showed stable water quality and water flux in highly saline feed solutions containing low surface tension substances.

In this study, glycidyl POSS was modified first by L-cysteine (as an amino acid) for fabrication of (L-cysteine functionalized POSS) nanoparticles by introducing hydroxyl, carboxyl, and amine functional groups to POSS structure. Then, the prepared L-cysteine functionalized POSS nanoparticles were applied to fabrication of [L-cysteine POSS-TiO_2] composite nanoparticles. The synthesized composite nanoparticles were then applied to preparing PEI/L-cysteine POSS-TiO_2 NF membranes. The prepared membranes were characterized by FTIR, FESEM and AFM analysis. The separation performance of fabricated membranes also was examined by pure water flux and rejection of Na_2SO_4, $Pb(NO_3)_2$, $CrSO_4$, and $Cu(NO_3)_2$ aqueous solutions.

EXPERIMENTAL

1. Materials and Methods

The octaglycidyloxypropyl-silsesquioxane (glycidyl-POSS) was supplied by Iran Polymer and Petrochemical Institute. Polyetherimide (PEI) (M_w=35,000 Da) was obtained from Sigma Aldrich. Tetrahydrofuran (THF), N, N-dimethylacetamide (DMAc) was purchased from DAEJUNG, Korea as a solvent. The L-cysteine was provided by AIP Co., Iran. The polyvinylpyrrolidone (PVP) as pore-forming was purchased from Merck.

2. L-cysteine POSS-TiO_2 Nanoparticles Synthesis

The modification of glycidyl-POSS by L-cysteine was according to Chang et al. [27] method. Briefly, glycidyl-POSS (1 mmol) was dissolved in 10 ml THF under N_2 purging. After stirring vigorously for 1 h at 50 °C, 1.0 g of L-cysteine (3.7 mmol) was added to the POSS solution for obtaining a clear solution. In the following of the process, the reaction between glycidyl group and thiol group

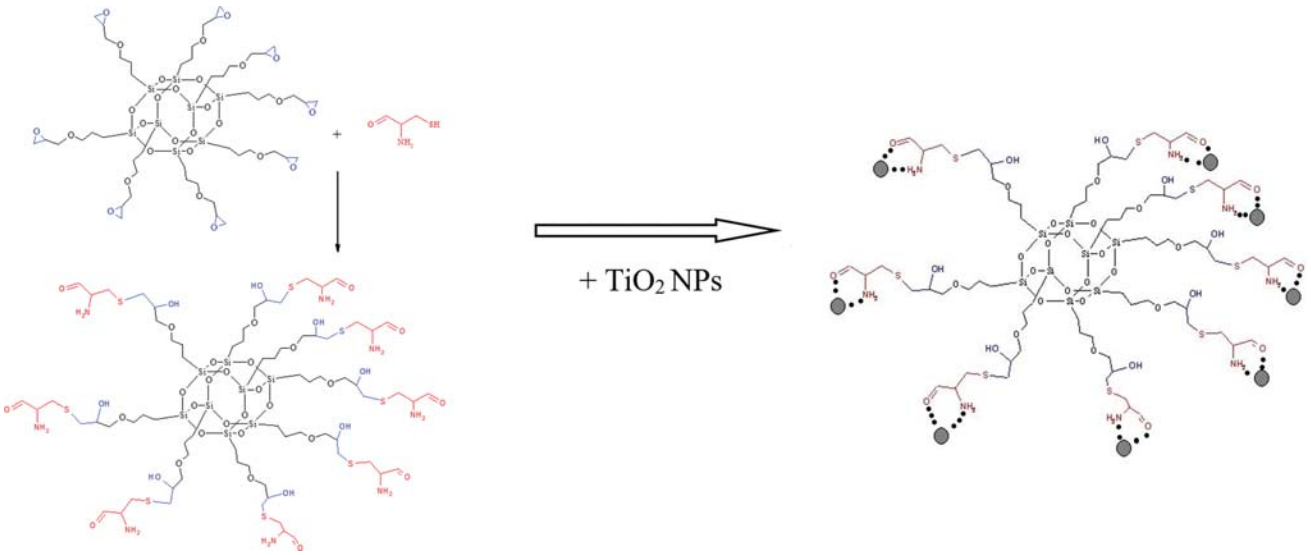

Fig. 1. The proposed mechanism for preparation of L-cysteine POSS-TiO_2 nanoparticles.

was complete by stirring for 5 h at 50 °C. Then, the solvent was removed by evaporation at room temperature for 24 h and dried in a vacuum oven at 50 °C for 12 h to isolate the modified-POSS. Finally, this product was washed with distilled water at 50 °C to remove unreacted L-cysteine. Fig. 1 shows the proposed mechanism for nanoparticle preparation. In the synthesis following, the synthesized nanoparticles from the prior step and TiO_2 were added to THF as a solvent and stirred for 12 h at 50 °C. After evaporation of the solvent, L-cysteine POSS-TiO_2 nanoparticles were dried in an oven for 12 h at 50-60 °C.

3. Membrane Preparation

The nanofiltration membranes were prepared by the phase inversion method. The blend of PEI/L-cysteine POSS-TiO_2 membranes with 18 wt% of PEI and 1 wt% of PVP was dissolved into the DMAc and stirred for 6 h. Different concentrations of L-cysteine POSS-TiO_2 composite nanoparticles were added to the polymeric solution in the prior section and stirring was continued for another 4 h. Then the casting solution was sonicated 1 h for better dispersion of nanoparticles. After removing air bubbles from the homogeneous solution during the 6 h, the prepared solution was cast on a glass plate with an applicator. Then the cast membranes were soaked into the deionized water for complete phase inversion process. The fabricated membranes were coded with M0, M1, M2, M3, and M4 in 0, 0.001, 0.01, 0.1, and 1 wt% of L-cysteine POSS-TiO_2 composite nanoparticles. Table 1 shows the solution composition details for the preparation of membranes.

4. Characterization Methods

The Fourier transform infrared spectroscopy (FTIR) with a Bruker spectrometer (TENSOR 27) was used to confirm the fabrication of L-cysteine POSS-TiO_2 composite nanoparticles and the presence of them into the membranes. Field emission scanning electron microscopy (FESEM) (MAIA3 model with accelerating voltage of 50 eV) was used for morphology investigation of fabricated membranes and synthesized L-cysteine POSS-TiO_2 composites nanoparticles. Moreover, the roughness and surface morphology of membranes were investigated by atomic force microscope (AFM) (FemtoScan model made in Russia) with scanning area 6 μm×6 μm.

Membrane porosity was calculated by dry-wet weight method. The wet weight of membranes was measured by membranes soaking in distilled water for 24 h. The dry weight of membranes was obtained by drying wet membranes in an oven at 60 °C for 24 h. The membrane porosity (ε) was measured by Eq. (1):

$$\varepsilon(\%) = \left(\frac{W_w - W_d}{\rho_f V_m}\right) \times 100 \quad (1)$$

where the dry weight and wet membrane are W_d, W_w (g). V_m and ρ_f are membrane volume (cm^3) and water density (g/cm^3), respectively. All experiments were carried out three times and the average values of results were considered for decreasing experimental errors.

Guerout-Elford-Ferry equation was used to obtain the mean pore size of membranes [1,31,32]:

$$r_m = \sqrt{\frac{(2.9 - 1.75\varepsilon)8\eta LQ}{\varepsilon A \Delta p}} \quad (2)$$

where η is the water viscosity (8.9×10^{-4} Pa·s), Q is the flow rate of the permeated pure water (m^3/s), and ΔP is operating pressure (0.45 MPa), A is the membrane filtration area (m^2), ε is the membrane porosity, and l is the membrane thickness (m).

The contact angle (θ) of prepared membranes was measured by using a contact angle measuring instrument (G10, Kruss, Germany) for the investigation of membrane hydrophilicity by deionized water. The water content of membranes was measured by Eq. (3) [13,33]:

$$\text{Water Content}(\%) = \left(\frac{W_w - W_d}{W_w}\right) \times 100 \quad (3)$$

where W_w and W_d are wet and dry weights of the prepared membranes, respectively.

5. Membrane Filtration Performance

The cross-flow nanofiltration system was used to investigate the performance of fabricated membranes. The membrane testing was at ambient temperature and 4.5 bar. Before the test of membranes, the membrane compaction was done with deionized water for 1 h and 5 bar to obtain steady state condition. The pure water flux (PWF) was determined by:

$$J_{w,1} = \frac{V}{A \times t} \quad (4)$$

where $J_{w,1}$ is the permeate flux ($Lm^{-2}h^{-1}$), V is the volume of permeate solution, A is the effective area of membrane (11.94 cm^2), and t is time (h).

The aqueous solution of Na_2SO_4, $Pb(SO_3)_2$, $CrSO_4$ and $Cu(NO_3)_2$ was used as feed solution for evaluation of nanofiltration membrane performance with concentrations 1,100 mg/L and 500 mg/L, respectively.

The salt rejection was measured by Eq. (5):

$$R(\%) = f\left(1 - \frac{C_p}{C_f}\right) \times 100 \quad (5)$$

where C_f and C_p are the concentration of feed solution and permeate, respectively.

Table 1. The used solution composition detail for membrane preparation

Membrane	PEI (wt%)	L-cysteine POSS-TiO_2 (wt%)	PVP (wt%)	DMAc (wt%)
M0	18	0	1	81%
M1	18	0.001%	1	80.999%
M2	18	0.01%	1	80.99%
M3	18	0.1%	1	80.9%
M4	18	1%	1	80

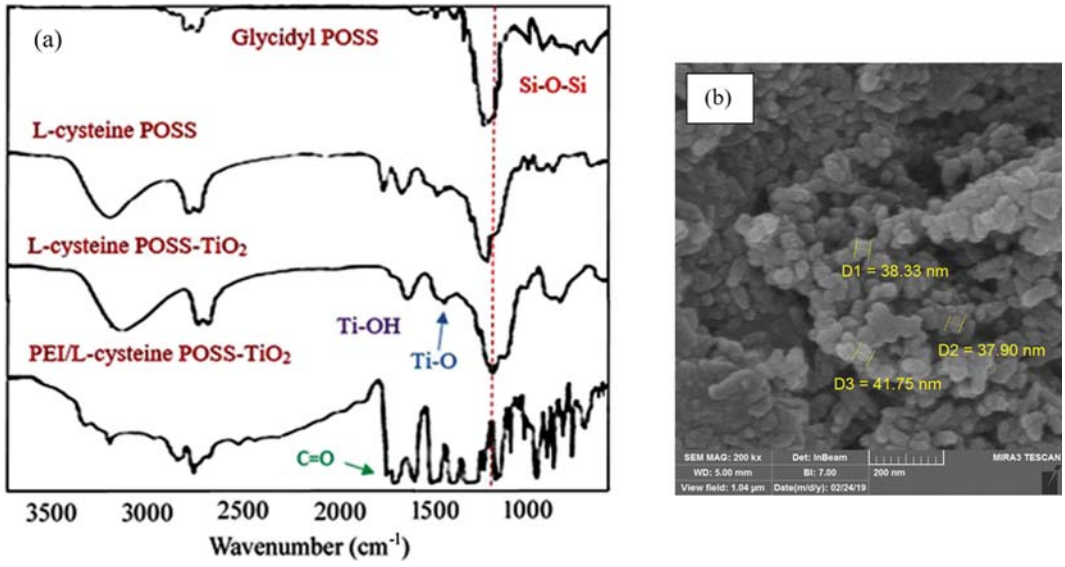

Fig. 2. The (a) FTIR analysis of composite nanoparticles and fabricated membrane containing of composite nanoparticles, and (b) FESEM image of L-cysteine POSS-TiO_2 composite nanoparticles.

After that, fouled membranes were placed into the deionized water for 2 h and then washed. Then, the pure water flux ($J_{w,2}$ (L/m^2h)) was obtained for measurement of the flux recovery ratio (FRR%):

$$FRR\% = \left(\frac{J_{w,2}}{J_{w,1}}\right) \times 100 \quad (6)$$

To minimize the experimental error, measurements were done three times for each sample and then their average value reported.

RESULT AND DISCUSSION

1. Membrane and Nanoparticle Characterization

The FTIR analysis of composite nanoparticles and fabricated membranes is shown in Fig. 2. The strong peak at 1,100 cm^{-1} and 1,074 cm^{-1} was attributed to present Si-O-Si bonds in all FTIR spectra due to the cage structure of POSS. The FTIR spectra for L-cysteine POSS, L-cysteine POSS-TiO_2 composite nanoparticles showed the hydroxyl and NH_2 groups into the nanoparticle structure [26,34,35]. Moreover, the adsorption peaks in 1,640 and 1,400-1,500 cm^{-1} are due to Ti-OH and Ti-O bonds in L-cysteine POSS-TiO_2 composite nanoparticles [36]. For PEI/L-cysteine POSS-TiO_2 membrane, the stretching vibration of 1,730 and 1,777 cm^{-1} is attributed to C=O symmetric and asymmetric carbonyl groups into the imide ring of PEI. The peak at 1,227 cm^{-1} related to the aromatic ether linkage (C-O-C) of PEI. The broad absorption peak around 3,000-3,600 cm^{-1} is related to the stretching of hydroxyl functional groups (-O-H) [33,37]. Introducing L-cysteine POSS-TiO_2 composite nanoparticles as additives in the PEI as membrane matrix led to chemical cross-linking by -NH_2 in nanoparticles and imide rings of PEI. The peak at 3,483 cm^{-1} is related to the presence of N-H groups. The N-H groups are due to the interaction between amine groups (-NH_2) in L-cysteine POSS-TiO_2 and imide rings in PEI. The FESEM image of L-cysteine POSS-TiO_2 composite nanoparticles shown in Fig. 2 confirmed the size of composite nanoparticles ~39.33 nm.

The FESEM images of the fabricated membranes are shown in Fig. 3 and Fig. 4. The asymmetric structure of membranes, including selective layer and a porous layer as membrane supporter with figure-like structure, is clear in all FESEM images. By incorporation of nanoparticles, the porous layer of membranes shifted to longer pores in PEI/L-cysteine POSS-TiO_2 membranes due to more hydrophilic groups on the surface of these membranes, thus leading to more interaction with water molecules. The size of voids increased in a high concentration of nanoparticles. Because by increasing hydrophilic nanoparticles, the interaction between membrane matrix and nanoparticles reduced and the interaction among nanoparticles and water molecules increased, and thus improved the exchange rate of solvent-water and rapid demixing that led to forming higher pores into the membrane structure [38-40]. The larger pores were observed for composite nanoparticles due to more speed in the exchange between solvent and non-solvent and nanoparticle migration to the membrane surface [13,39]. It should be considered that the cage structure of POSS into the composite nanoparticles can lead to tuning pores into the membrane structure [41-44]. Also, the thickness of selective layer was enhanced by increasing nanoparticles compared to the pristine PEI membrane, which is an important factor for salt separation [45]. As is clear in FESEM images, the selective layer thickness of PEI/TiO_2 membrane is higher than PEI/L-cysteine POSS-TiO_2 membrane. This can be described due to lower accumulation of L-cysteine POSS-TiO_2 nanoparticles and better affinity with membrane structure that was obtained by hydrophilic groups such as hydroxyl, carboxyl, and amine. By incorporation of nanoparticles, the selective layer thickness increased and the highest thickness selective layer was obtained for M3 by incorporation 0.1 wt% of TiO_2 and L-cysteine POSS-TiO_2 nanoparticles.

The surface morphology of fabricated membranes was investi-

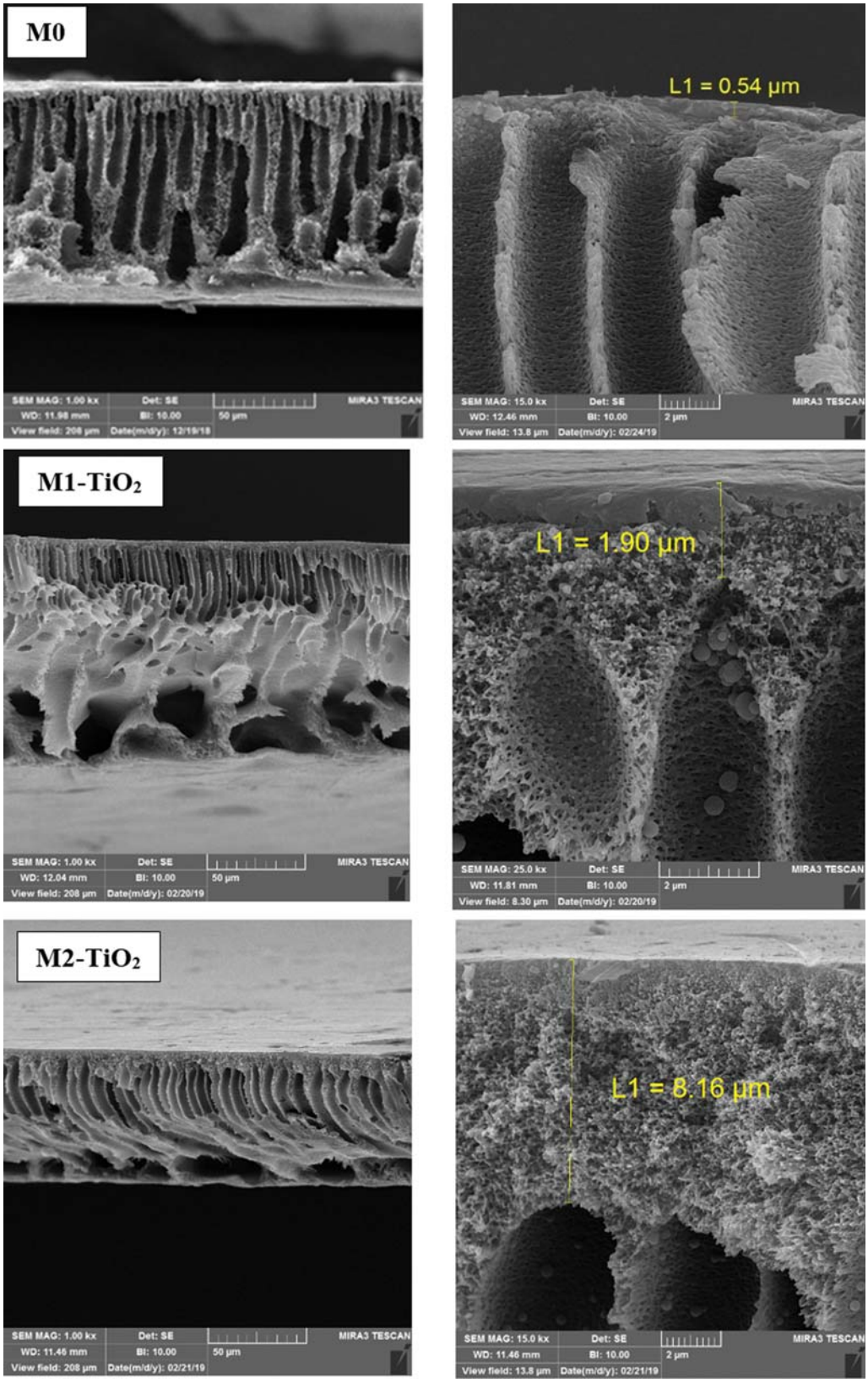

Fig. 3. The cross sectional FESEM image of PEI/TiO_2 blended membranes.

gated by AFM analysis in the scanning area 6 µm×6 µm as shown in Fig. 5. Moreover, the roughness parameter of PEI/L-cysteine POSS-TiO_2 membranes is clear in Table 2. By incorporation of nanoparticles, average roughness (R_a) of membranes and the max-

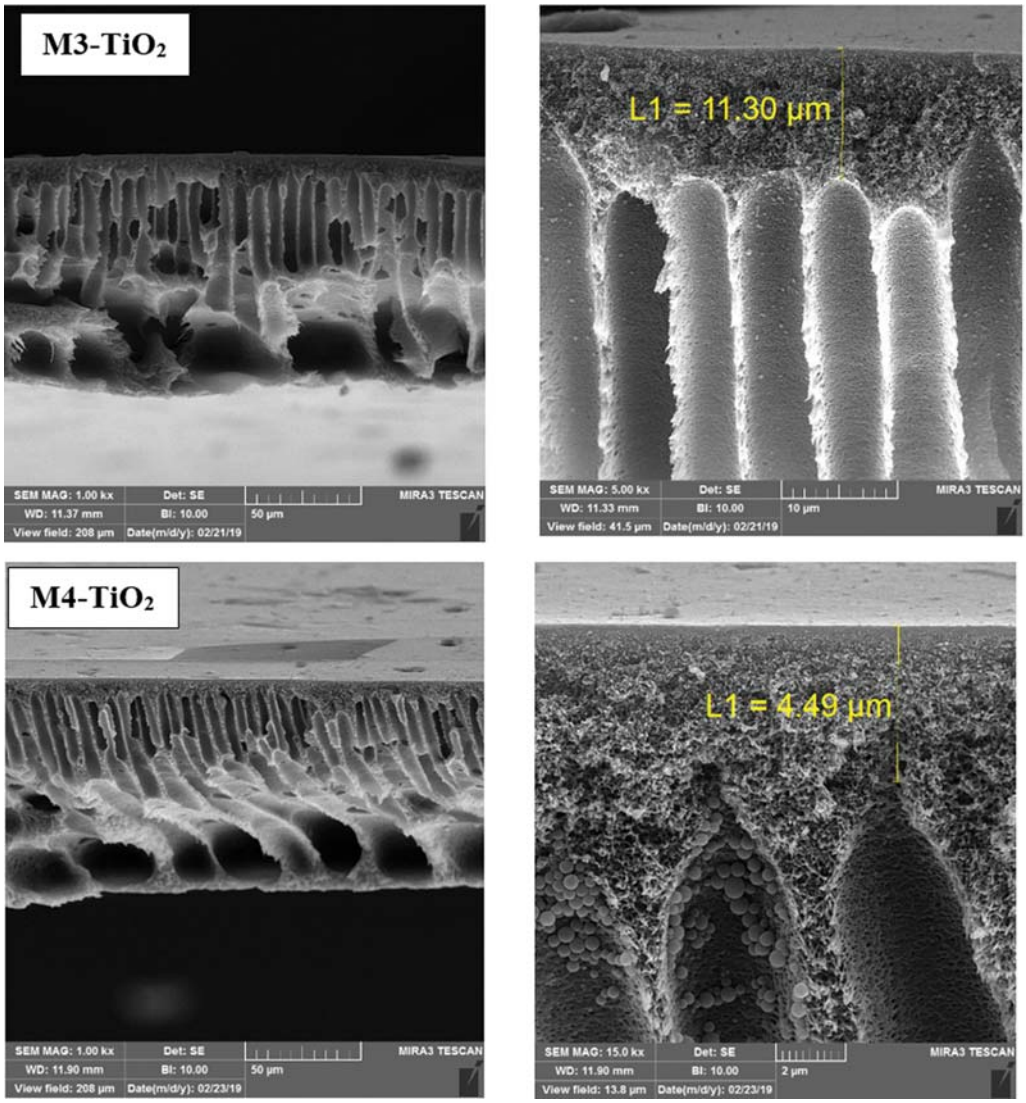

Fig. 3. Continued.

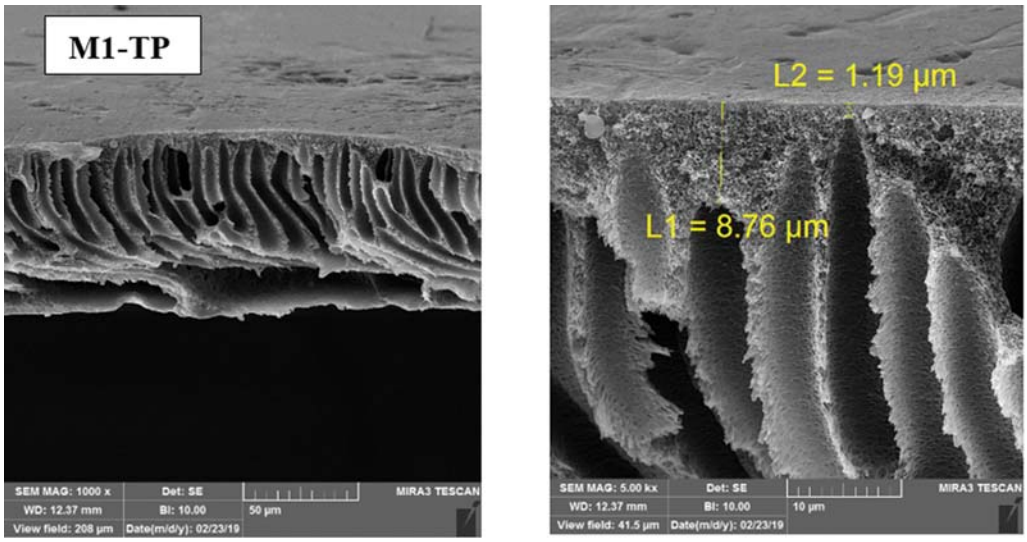

Fig. 4. The cross-sectional FESEM images of PEI/L-cysteine POSS-TiO_2 membranes.

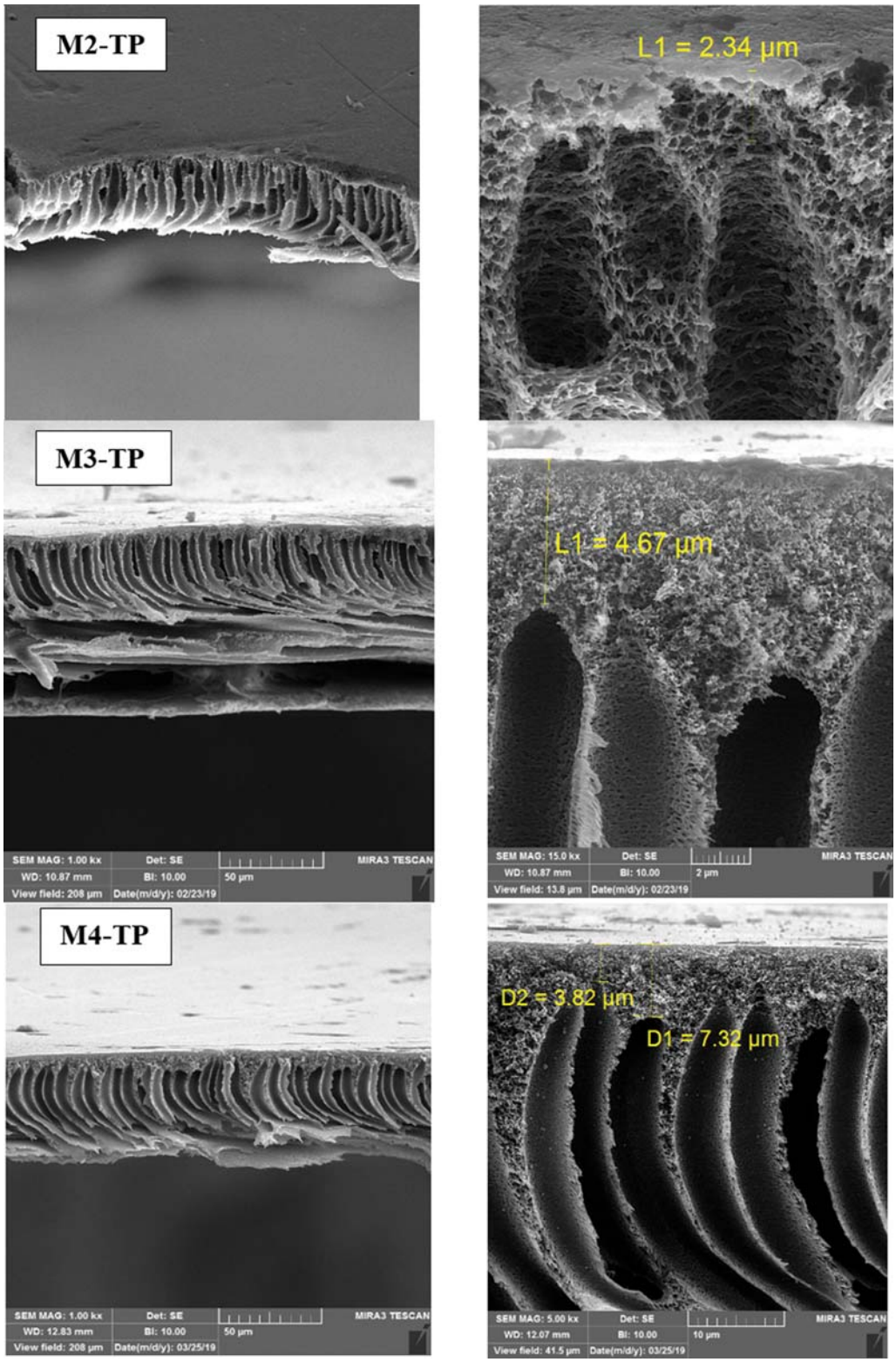

Fig. 4. Continued.

imum height of roughness (R_{max}) decreased compared with the pristine PEI due to filling cavities with hydrophilic composite nanoparticles and forming smoother surface. M3 showed the lowest surface roughness (R_a=1 nm) and R_a reduced from 19.49 nm for the pristine PEI to 1 nm for 0.1 wt% particles due to filling pores with additives. Therefore, incorporation of nanoparticles into the membrane enhanced antifouling properties [46-49]. But R_a increased to 3.2 nm for membranes containing 1 wt% of composite nanopar-

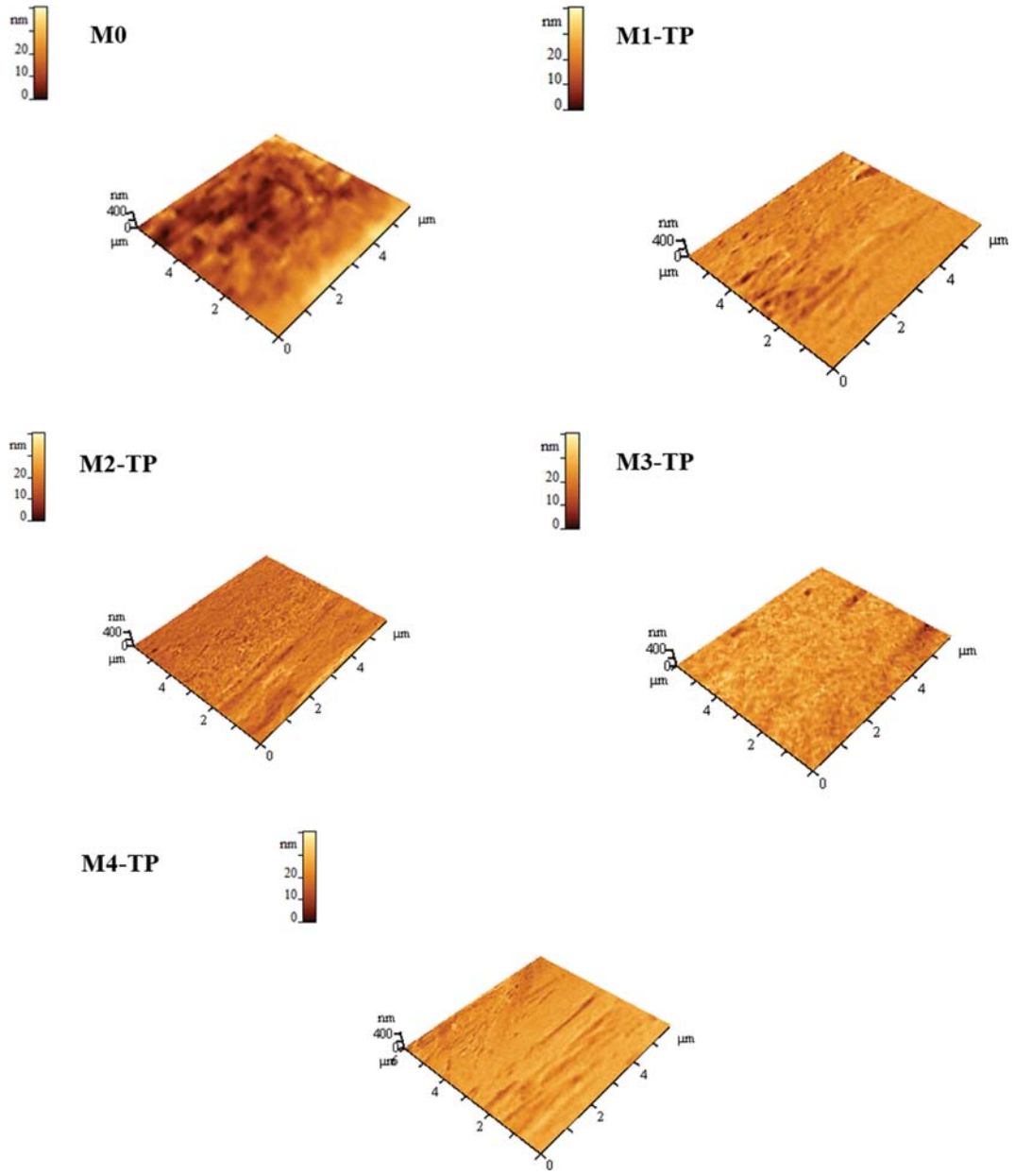

Fig. 5. The AFM images of fabricated membranes.

Table 2. The roughness parameter of PEI/L-cysteine POSS-TiO_2 membranes

Membrane No.	R_a (nm)	R_{max} (nm)
M0	19.49	84.36
M1	2.7	14.66
M2	2.62	10.37
M3	1	5.9
M4	3.2	18.21

ticles. The increasing surface roughness was attributed to composite nanoparticle aggregation on the membrane surface that can lead to pore blockage and form a rougher membrane surface.

2. Membrane Filtration Performance

The hydrophilic groups on the composite nanoparticles improved the membrane hydrophilicity. The contact angle of the fabricated membranes (Fig. 6) showed the improvement of membrane hydrophilicity with the incorporation of TiO_2 and L-cysteine POSS-TiO_2 composite nanoparticles. By incorporation of TiO_2 and L-cysteine POSS-TiO_2 nanoparticle, the contact angle decreased from 65° in the pristine membrane to 30° in M4 due to the presence of hydrophilic groups in the nanoparticles. The hydrophilic groups into nanoparticles increased water transport via the membrane. As shown in the Fig. 7, the pure water flux of PEI/TiO_2 membranes was lower than pristine PEI membrane, while by introducing L-cysteine POSS-TiO_2 composite nanoparticles improved to 22.03 (L/m^2h) for M4 in 1 wt% composite nanoparticles, that is the result of increasing

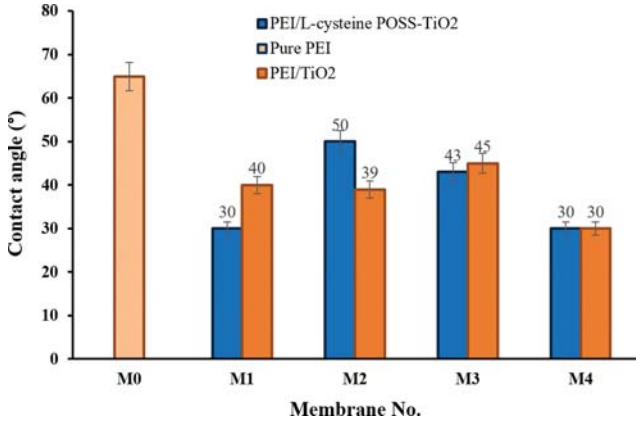

Fig. 6. The contact angle of fabricated membranes.

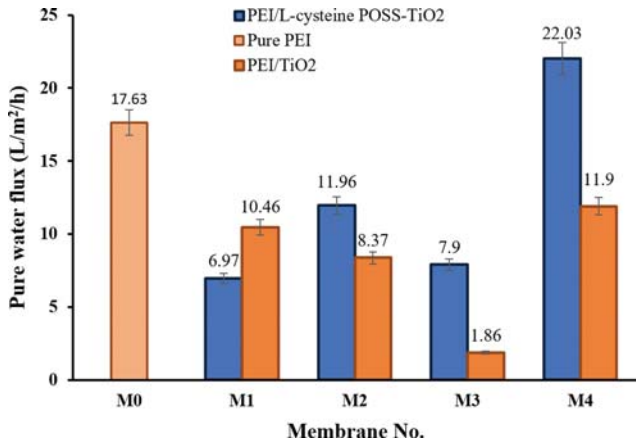

Fig. 7. The pure water flux for all fabricated membranes.

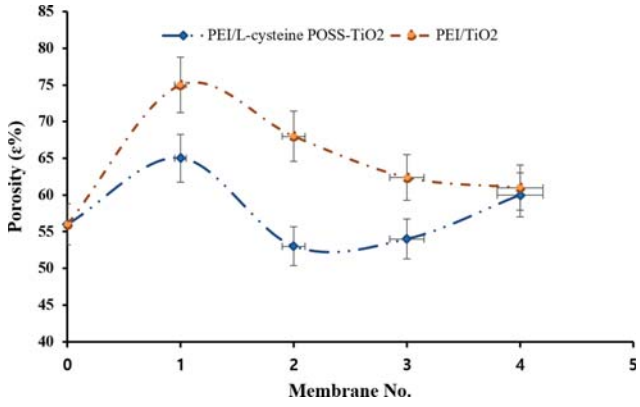

Fig. 8. The porosity of fabricated membranes.

membrane hydrophilicity and higher affinity of particles with polymer matrix and thus better nanoparticle dispersion compared with TiO_2 nanoparticles. These results are in agreement with membrane porosity (Fig. 8) and the mean pore size of membranes (Fig. 9). As shown in Fig. 8 and Fig. 9 the porosity and mean pore size of membrane decreased due to filling pores with nanoparticles and then increased in a high concentration of nanoparticles. The FESEM

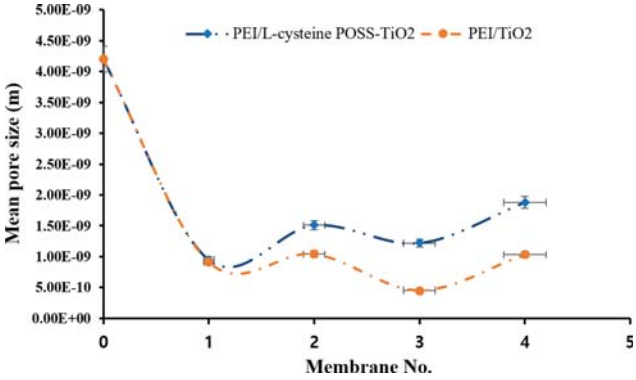

Fig. 9. Mean pore size of all fabricated membranes.

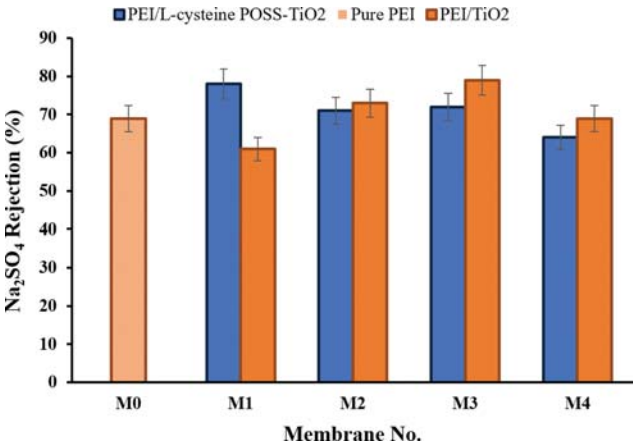

Fig. 10. The Na_2SO_4 rejection for the fabricated membranes at feed concentration of 1,000 mg/L.

images of membranes confirm these results.

The membrane separation was examined by the aqueous solution of Na_2SO_4, $Pb(NO_3)_2$, $CrSO_4$, $Cu(NO_3)_2$. Fig. 10 shows the Na_2SO_4 rejection of fabricated membranes. The Na_2SO_4 rejection improved from 69% in pure PEI to 78% in M1 due to presence of negative charges on the membrane surface and electrostatic repulsion of SO_4^{2-} ions. Furthermore, the cage structure of POSS affected the size of porosities and led to tuning porosities into the membrane structure [18,50,51]. On the other hand, the lowest PWF was obtained at M1-TP, which led to reduced salt ion transport with water molecules. However, the membrane porosity increased in M1-TP, but the mean pore size of the membrane decreased, which prohibited water molecules and salt ion transport. The highest Na_2SO_4 rejection (79%) was obtained for 0.1 wt% TiO_2 nanoparticles into the PEI membrane (M3). Decreasing membrane porosity, decreasing mean pore size of membrane and increasing the selective layer thickness to 11.3 μm are effective in salt ion rejection. Moreover, electrostatic repulsion between negative charges on the membrane surface and SO_4^{2-} is the major mechanism for Na_2SO_4 rejection. By comparison between PEI/TiO_2 and PEI/L-cysteine POSS-TiO_2 in Na_2SO_4 rejection with values of 79% and 78%, respectively, it was found that the POSS particles have not a significant effect on the Na_2SO_4 rejection, and electrostatic repul-

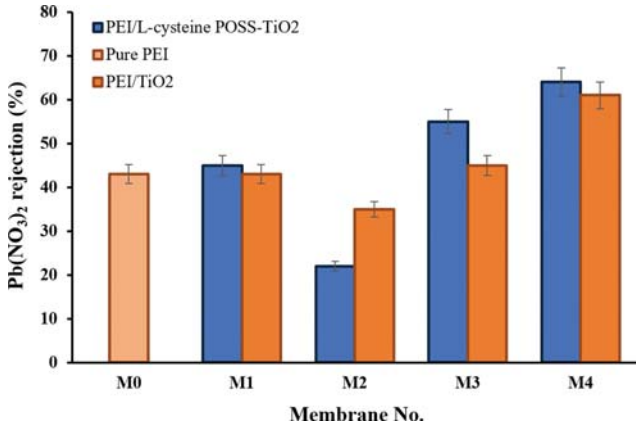

Fig. 11. $Pb(NO_3)_2$ rejection of fabricated membranes at feed concentration of 500 mg/L.

sion is an important mechanism for Na_2SO_4 rejection. Furthermore, the decline of Na_2SO_4 rejection was related to the accumulation of nanoparticles and the decrease of functional group effects on the membrane surface for ion repulsion.

The separation performance of $Pb(NO_3)_2$ is shown in Fig. 11. As is clear, by incorporation of composite nanoparticles, the $Pb(NO_3)_2$ rejection improved from 43% in M0 to 64% in M4. The cage structure of POSS has a high potential for adsorption of Pb^{2+} ions [24, 52,53]. However, the NO_3^- repulsion by negative charges on the membrane surface is another reason for lead rejection. PEI/TiO_2 membranes enhanced the lead rejection to 61% in 1 wt% nanoparticles. As is clear in Fig. 11, the presence of POSS particles into the membrane structure improved the lead rejection due to the adsorption mechanism by the cage structure of POSS. Larger mean pore sizes in PEI/L-cysteine POSS-TiO_2 membranes increased the active sites for adsorption of Pb^{2+} ions. Moreover, the reduction of Pb^{2+} rejection in M2 membrane can be explained by longer finger-like structure (see FESEM in Fig. 3 and Fig. 4).

Investigation of $CrSO_4$ rejection (Fig. 12) by TiO_2 and L-cysteine POSS-TiO_2 particles showed good performance of nanocomposite particles to Cr^{2+} rejection. By considering negative charges on the membrane surface and SO_4^{2-} repulsion by membranes surface, the adsorption mechanisms by POSS in composites nanoparticles is important for Cr^{2+} rejection. The highest $CrSO_4$ rejection (67%) was found for M3-TP. M3-TP showed the highest selective layer thickness (4.67 μm). But in a high concentration of composite nanoparticles, decreased the Cr^{2+} rejection that can be explained by high porosity, longer and larger mean pore size of membrane, and thus high PWF that leads to from nonselective pores and more aqueous solution transport. Furthermore, introducing TiO_2 nanoparticles into the membrane, Cr^{2+} rejection was reduced from 62% to 32%. It was considered that the addition of decreasing PWF compared with the pristine PEI membrane; increasing TiO_2 nanoparticles has a negative effect on Cr^{2+} rejection due to reducing the mean pore size of the membrane, more aggregation of TiO_2 nanoparticles in the membrane structure and thus reduction of active sites to adsorption of Cr^{2+} ions.

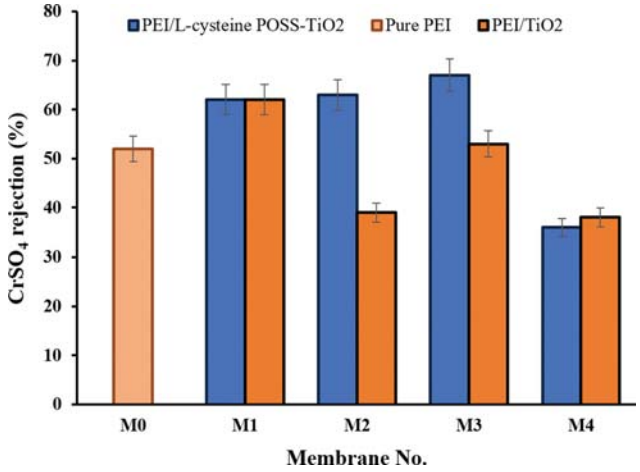

Fig. 12. $CrSO_4$ rejection of fabricated membranes at feed concentration of 500 mg/L.

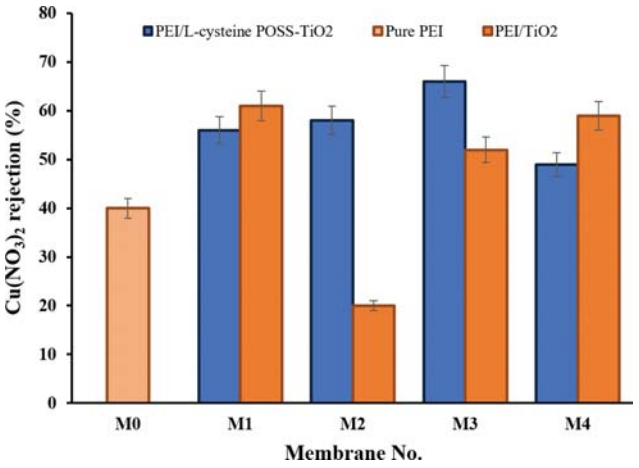

Fig. 13. $Cu(NO_3)_2$ rejection of fabricated membranes at feed concentration of 500 mg/L.

The rejection of $Cu(NO_3)$ is shown in Fig. 13. As is clear, incorporation of L-cysteine POSS-TiO_2 composite nanoparticles improved Cu^{2+} rejection from 40% in M0 to 66% in M3-TP. However, introducing TiO_2 nanoparticles increased Cu^{2+} rejection to 61% in M1-TiO_2, but low PWF of PEI/TiO_2 membrane decreased separation performance of these membranes. Moreover, the Cu^{2+} rejection decreased by increasing TiO_2 nanoparticles from M1-TiO_2 to M4-TiO_2 and that can be the result of decreasing more active sites for Cu^{2+} adsorption. Because, the membrane pores fill with TiO_2 nanoparticles. Furthermore, by increasing L-cysteine POSS-TiO_2 nanoparticles increased Cu^{2+} rejection due to the presence cage structure of POSS and the formation of more active sites for Cu^{2+} adsorption. Then, the Cu^{2+} rejection was reduced in 1 wt% composite nanoparticles due to nanoparticle aggregation and lower active sites.

The comparison between separation performance of fabricated membranes in this study with several related researches in Na_2SO_4, $Pb(NO_3)_2$, $Cu(NO_3)_2$ and $CrSO_4$ removal is shown in Table 3. As seen, the modified membranes in the current study are comparable with that of other reported ones.

The flux recovery ratio (FRR%) of M0 and M3-TiO_2 and M3-

Table 3. Comparison between the separation performances of prepared membranes in this study with some related researches

Membrane	Nanoparticle	Nanoparticle loading (wt%)	Feed concentration (mg/L)	Pressure (bar)	PWF	Rejection (%)				Ref.
						Na^{2+}	Pb^{+2}	Cu^{+2}	Cr^{2+}	
Polyether sulfone	GO[a]	1	1,000	5	7.3 ($kg/m^2 \cdot h$)		-	77	-	[54]
Polyether sulfone	PANI/Fe_3O_4[b]	0.1	20	5	47 ($kg/m^2 \cdot h$)		-	85	-	[55]
PI84	GO	0.9	0.05 M	15	13.07 (L/m^2h)	100	-	-	-	[56]
Poly(phenylene ether-ether sulfone)	TiO_2	0.1	1,000	6	44 (L/m^2h)	74	-	-	-	[13]
PVC-ABA/PSf		0.5	10	4.5	34.17 (L/m^2h)	-	68	-	-	[57]
PVDF	A-HNTs[c]	0.66	100	-	26 (L/m^2h)	-	-	47	-	[58]
PEI	TiO_2	1	1,000	4.5	11.9 (L/m^2h)	69	-	-	-	In this study
			500			-	61	-	-	
			500			-	-	59	-	
			500			-	-	-	38	
PEI	L-cysteine POSS-TiO_2	0.1	1,000	4.5	7.9 (L/m^2h)	72	-	-	-	In this study
			500			-	55	-	-	
			500			-	-	66	-	
			500			-	-	-	67	

[a]Graphene oxide (GO).
[b]Polyaniline/iron (II, III) oxide (PANI/Fe_3O_4) nanoparticles.
[c]3-Aminopropyltriethoxysilane (APTES) grafted halloysite nanotubes (HNTs).

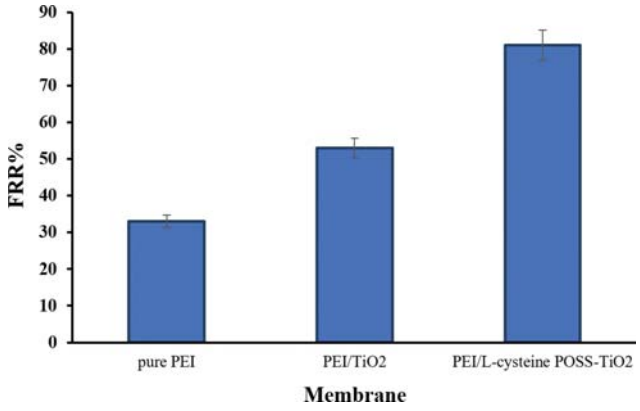

Fig. 14. FRR% ratio of pure PEI, PEI/TiO_2 and PEI/L-cysteine POSS-TiO_2 (0.1 wt%) membranes.

TP membranes is illustrated in Fig. 14. Generally, FRR% of all prepared membranes increased compared with pristine PEI membrane, and the highest FRR% was 53% and 81% in 0.1 wt% TiO_2 and composite nanoparticles, respectively. The improvement of FRR% was related to present functional groups -OH, -COOH on the membrane surface and decreasing membrane roughness according to AFM results for M3 membranes. Also, increasing the selective layer thickness and formation of dense layer structure on the membrane surface is effective for improvement of anti-fouling properties. FRR% shows the ability of membrane recycling after fouling. Membrane hydrophilicity is the most important factor to decrease fouling. However, POSS materials are hydrophobic, but the modification of POSS with different functional groups such as -OH, -COOH and -NH_2 enhanced the hydrophilicity of POSS nanoparticles.

CONCLUSION

Glycidyl-POSS was functionalized by L-cysteine to synthesis of L-cysteine/POSS nanoparticles containing of hydroxyl, carboxyl, and amine groups. Then, the synthesized nanoparticles were applied to fabrication of L-cysteine POSS-TiO_2 composite nanoparticles. The synthesized (L-cysteine POSS-TiO_2) nanoparticles were then applied to preparing of PEI based NF membranes. The used composite nanofiller showed potential of POSS-based nanoparticles for the enhancement of pure water flux and separation performance of NF membranes. The rejection of Na_2SO_4 promoted ~11% compared with the pristine PEI membrane in 0.1 wt% nanoparticles, and $Pb(NO_3)_2$ rejection increased ~33% compared with pristine PEI membrane in 1 wt% nanoparticles. Moreover, $CrSO_4$, and $Cu(NO_3)_2$ removal was enhanced 22%, and 39% compared with

pristine PEI membrane, respectively. The hydrophilic groups in composite nanoparticles enhanced anti-fouling properties of the prepared membranes, and the best FRR% (81%) was obtained for M3 with 0.1 wt% of composite nanoparticles.

REFERENCES

1. A. Rahimpour, *Desalination*, **265**, 93 (2011).
2. E. Bagheripour, A. Moghadassi and S. Hosseini, *Int. J. Eng.*, **29**(3), 280 (2016).
3. D. Rana and T. Matsuura, *Chem. Rev.*, **110**, 2448 (2010).
4. D. J. Miller, D. R. Dreyer, C. W. Bielawski, D. R. Paul and B. D. Freeman, *Angew. Chem. Int. Ed.*, **56**, 4662 (2017).
5. S. M. Hosseini, M. Afshari, A. R. Fazlali, S. Koudzari Farahani, S. Bandehali, B. Van der Bruggen and E. Bagheripour, *Chem. Eng. Res. Design*, **147**, 390 (2019).
6. A. Azari, R. Rezaei and H. Sanaeepur, *Desalination Water Treatment*, **124**, 308 (2018).
7. S. Bandehali, A. Moghadassi, F. Parvizian, S. M. Hosseini, T. Matsuura and E. Joudaki, *J. Energy Chem.*, **46**, 30 (2020).
8. M. Zhang, K. Guan, Y. Ji, G. Liu, W. Jin and N. Xu, *Nat. Commun.*, **10**, 1253 (2019).
9. H.-Z. Zhang, Z.-L. Xu and J.-Y. Sun, *RSC Adv.*, **8**, 29455 (2018).
10. M. Maarefian, S. Bandehali, S. Azami, H. Sanaeepur and A. Moghadassi, *Int. J. Energy Res.*, **43**, 8217 (2019).
11. S. Bandehali, A. Kargari, A. Moghadassi, H. Saneepur and D. Ghanbari, *Asia-Pacific J. Chem. Eng.*, **9**, 638 (2014).
12. B. Khorshidi, I. Biswas, T. Ghosh, T. Thundat and M. Sadrzadeh, *Scientific Rep.*, **8**, 784 (2018).
13. P. Mobarakabad, A. Moghadassi and S. Hosseini, *Desalination*, **365**, 227 (2015).
14. M. Jyothi, V. Nayak, M. Padaki and R. G. Balakrishna, *J. Photochem. Photobiol. A: Chem.*, **339**, 89 (2017).
15. S. S. Hosseini, A. Nazif, M. A. A. Shahmirzadi and I. Ortiz, *Sep. Purif. Technol.*, **187**, 46 (2017).
16. E. Ayandele, B. Sarkar and P. Alexandridis, *Nanomaterials*, **2**, 445 (2012).
17. Y. He, Y. P. Tang and T. S. Chung, *Ind. Eng. Chem. Res.*, **55**, 12929 (2016).
18. X. You, H. Wu, Y. Su, J. Yuan, R. Zhang, Q. Yu, M. Wu, Z. Jiang and X.-Z. Cao, *J. Mater. Chem. A*, **6**, 13191 (2018).
19. H. Sanaeepur, A. E. Amooghin, S. Bandehali, A. Moghadassi, T. Matsuura and B. Van der Bruggen, *Prog. Polym. Sci.*, **90**, 80 (2019).
20. H. Sanaeepur, A. Ebadi Amooghin and S. Bandehali, *Theoretical gas permeation models for mixed matrix membranes*, LAP LAMBERT Academic Publishing, Beau Bassin, Mauritius (2018).
21. M. Rezakazemi, A. Ebadi Amooghin, M. M. Montazer-Rahmati, A. F. Ismail and T. Matsuura, *Prog. Polym. Sci.*, **39**, 817 (2014).
22. A. E. Amooghin, S. Mashhadikhan, H. Sanaeepur, A. Moghadassi, T. Matsuura and S. Ramakrishna, *Prog. Mater. Sci.*, **102**, 222 (2018).
23. N. L. D. Filho, F. Marangoni and R. M. Costa, *J. Colloid Interface Sci.*, **313**, 34 (2007).
24. K. Xie, L. Jing, W. Zhao and Y. Zhang, *J. Appl. Polym. Sci.*, **122**, 2864 (2011).
25. X. You, T. Ma, Y. Su, H. Wu, M. Wu, H. Cai, G. Sun and Z. Jiang, *J. Membr. Sci.*, **540**, 454 (2017).
26. M. Dalwani, J. Zheng, M. Hempenius, M. J. Raaijmakers, C. M. Doherty, A. J. Hill, M. Wessling and N. E. Benes, *J. Mater. Chem. A*, **22**, 14835 (2012).
27. S. C. Chen, X. Z. Fu and T.-S. Chung, *Desalination*, **335**, 17 (2014).
28. J. Duan, E. Litwiller and I. Pinnau, *J. Membr. Sci.*, **473**, 157 (2015).
29. C. Lu, C. Su, H. Cao, X. Ma, F. Duan, J. Chang and Y. Li, *Mater. Lett.*, **228**, 85 (2018).
30. Y. W. Chang, E. Wang, G. Shin, J. E. Han and P. T. Mather, *Polym. Adv. Technol.*, **18**, 535 (2007).
31. Y. Mansourpanah, S. Madaeni, A. Rahimpour, A. Farhadian and A. Taheri, *J. Membr. Sci.*, **330**, 297 (2009).
32. E. Bagheripour, A. Moghadassi, S. Hosseini, B. Van der Bruggen and F. Parvizian, *J. Ind. Eng. Chem.*, **62**, 311 (2018).
33. R. S. Hebbar, A. M. Isloor, A. Ismail, S. J. Shilton, A. Obaid and H.-K. Fun, *New J. Chem.*, **39**, 6141 (2015).
34. Y. W. Chang, E. Wang, G. Shin, J. E. Han and P. T. Mather, *Polym. Adv. Technol.*, **18**, 535 (2007).
35. Y. Kinoshita, K. Wakimoto, A. H. Gibbons, A. P. Isfahani, H. Kusuda, E. Sivaniah and B. Ghalei, *J. Membr. Sci.*, **539**, 178 (2017).
36. A. León, P. Reuquen, C. Garín, R. Segura, P. Vargas, P. Zapata and P. A. Orihuela, *Appl. Sci.*, **7**, 49 (2017).
37. A. Sumisha, G. Arthanareeswaran, A. F. Ismail, D. P. Kumar and M. V. Shankar, *RSC Adv.*, **5**, 39464 (2015).
38. M. Moochani, A. Moghadassi, S. M. Hosseini, E. Bagheripour and F. Parvizian, *J. Chem. Eng.*, **33**, 2674 (2016).
39. E. Bagheripour, A. Moghadassi and S. M. Hosseini, *Korean J. Chem. Eng.*, **33**, 1462 (2016).
40. E. Bagheripour, A. Moghadassi and S. M. Hosseini, *Int. J. Eng.*, **30**, 821 (2017).
41. M. R. Esfahani, V. L. Pallem, H. A. Stretz and M. J. Wells, *Spectrochim. Acta Part A: Mol. Biomol. Spectrosc.*, **189**, 415 (2018).
42. W. Zhang, G. Camino and R. Yang, *Prog. Polym. Sci.*, **67**, 77 (2017).
43. K. Nusser, G. J. Schneider, W. Pyckhout-Hintzen and D. Richter, *Macromolecules*, **44**, 7820 (2011).
44. X. You, H. Wu, Y. Su, J. Yuan, R. Zhang, Q. Yu, M. Wu and Z. Jiang, X.-Z. Cao, *J. Mater. Chem. A*, **6**, 13191 (2018).
45. E. Fontananova, J. C. Jansen, A. Cristiano, E. Curcio and E. Drioli, *Desalination*, **192**, 190 (2006).
46. E. Bagheripour, A. Moghadassi, S. Hosseini, M. Ray, F. Parvizian and B. Van der Bruggen, *Chem. Eng. Res. Design*, **132**, 812 (2018).
47. A. Razmjou, J. Mansouri and V. Chen, *J. Membr. Sci.*, **378**, 73 (2011).
48. M. R. Mehrnia, Y. M. Mojtahedi and M. Homayoonfal, *Desalination*, **372**, 75 (2015).
49. M. Farjami, A. Moghadassi, V. Vatanpour, S. M. Hosseini and F. Parvizian, *J. Ind. Eng. Chem.*, **72**, 144 (2018).
50. S. Bandehali, F. Parvizian, A. R. Moghadassi and S. M. Hosseini, *J. Polym. Res.*, **26**, 211 (2019).
51. S. Bandehali, F. Parvizian, A. Moghadassi and S. M. Hosseini, *Sep. Purif. Technol.*, **237**, 116361 (2020).
52. S. Bandehali, A. Moghadassi, F. Parvizian, J. Shen and S. Hosseini, *Korean J. Chem. Eng.*, **37**, 263 (2020).
53. S. Bandehali, A. Moghadassi, F. Parvizian and S. Hosseini, *Korean J. Chem. Eng.*, **36**, 1657 (2019).
54. N. Gholami and H. Mahdavi, *Adv. Polym. Technol.*, **37**(8), 3529 (2018).
55. P. Daraei, S. S. Madaeni, N. Ghaemi, E. Salehi, M. A. Khadivi, R.

Moradian and B. Astinchap, *J. Membr. Sci.*, **415**, 250 (2012).
56. N. K. Zaman, R. Rohani, A. W. Mohammad and A. M. Isloor, *Chem. Eng. Sci.*, **177**, 218 (2018).
57. V. Nayak, M. Jyothi, R. G. Balakrishna, M. Padaki and S. Deon, *J. Hazard. Mater.*, **331**, 289 (2017).
58. G. Zeng, Y. He, Y. Zhan, L. Zhang, Y. Pan, C. Zhang and Z. Yu, *J. Hazard. Mater.*, **317**, 60 (2016).